AGU PUBLICATIONS

JGR

Journal of Geophysical Research: Space Physics

RESEARCH ARTICLE

10.1002/2013JA019705

Key Points:
- Thermospheric gravity wave maps for different seasons
- Similarity between thermospheric and stratospheric gravity wave distributions
- Observational constraints on gravity wave dynamics

Correspondence to:
J. Park,
park@gfz-potsdam.de

Citation:
Park, J., H. Lühr, C. Lee, Y. H. Kim, G. Jee, and J.-H. Kim (2014), A climatology of medium-scale gravity wave activity in the midlatitude/low-latitude daytime upper thermosphere as observed by CHAMP, *J. Geophys. Res. Space Physics*, *119*, 2187–2196, doi:10.1002/2013JA019705.

Received 11 DEC 2013
Accepted 20 FEB 2014
Accepted article online 24 FEB 2014
Published online 12 MAR 2014

A climatology of medium-scale gravity wave activity in the midlatitude/low-latitude daytime upper thermosphere as observed by CHAMP

J. Park[1], H. Lühr[1], C. Lee[2,3], Y. H. Kim[3], G. Jee[2], and J.-H. Kim[2]

[1]GFZ German Research Center for Geosciences, Potsdam, Germany, [2]Division of Climate Change, Korea Polar Research Institute, Incheon, South Korea, [3]Department of Astronomy and Space Science, Chungnam National University, Daejeon, South Korea

Abstract We report on a detailed global climatology of medium-scale (150–600 km) thermospheric gravity wave (GW) activity using mass density observations onboard the CHAMP satellite from 2001 to 2010. Our study focuses mainly on daytime (09–18 h in local time) and midlatitude/low-latitude upper thermosphere between 300 km and 400 km altitudes. Midlatitude GW activity is strongest in the winter hemisphere. GW activity during June solstice adjacent to the Andes and Antarctic Peninsula is stronger than in any other season or location. GW activity in the low-latitude summer hemisphere is stronger above continents than above oceans: especially during December solstice and equinoxes. In terms of relative density variation, GW activity is stronger during solar minimum than solar maximum. These results agree well with the characteristics of stratospheric GWs, implying that the CHAMP GWs are mainly caused by GWs from tropospheric/stratospheric processes. Using mesosphere/lower thermosphere wind observations at a Korean Antarctic station, we investigated at which altitudes the upper thermospheric GW climatology becomes visible. While the correlation is insignificant at $z = 82$–88 km, it becomes significant for most cases at $z = 90$–98 km, suggesting that the upper thermospheric GW climatology may start to emerge at $z \geq 90$ km.

1. Introduction

Since the advent of microwave/infrared imagers onboard satellites, the global climatology of gravity waves (GWs) has been intensively studied in the stratosphere (e.g., *Wu and Waters* [1996], *Wu*, [2004], *Jiang et al.* [2004], *Preusse et al.* [2006], and *John and Kumar* [2013], just to name a few). On a global map the primary maximum of GW activity appears at midlatitudes/high latitudes in the winter hemisphere, while a secondary peak shows up at low latitudes in the summer hemisphere [e.g., *Ern et al.*, 2011; *John and Kumar*, 2013]. The former has mostly been attributed to wind blocking by orography [e.g., *Jiang et al.*, 2004], while the latter in general originates from deep tropospheric convection [e.g., *McLandress et al.*, 2000]. The vertical wavelength of GWs is shorter at lower latitudes than at higher latitudes [*Alexander et al.*, 2008; *Wang and Alexander*, 2010]. As for midlatitude/high-latitude regions, the GW distribution around June solstice exhibits one clear peak adjacent to the Andes and the Antarctic Peninsula [e.g., *Wu*, 2004; *John and Kumar*, 2013], while the distribution near December solstice shows multiple peaks at various geographic longitude (GLON) sectors in the Northern Hemisphere [*McLandress et al.*, 2000; *Jiang et al.*, 2004]. Additionally, the GW activity around the Andes and Antarctic Peninsula during local winter is stronger than at any other location or season [*McLandress et al.*, 2000]. The stratospheric GW momentum flux, which reflects temperature fluctuation amplitudes normalized by the background temperature, is higher during solar minimum than during solar maximum [*Ern et al.*, 2011].

Several studies investigated global GW climatology at altitudes above the stratosphere. According to *John and Kumar* [2012], (1) the GW climatology maintains its stratospheric morphology up to about 80 km altitude, and (2) the average GW climatology between 80 km and 100 km is noticeably different from the stratospheric counterpart: the GW activity between 80 km and 100 km is stronger in the summer hemisphere than in the winter hemisphere. Similarly, *Ern et al.* [2011] reported that GW climatology at 70 km altitude is already very different from that in the stratosphere. Therefore, the GW climatology seems to undergo substantial changes in morphology between 70 and 100 km, that is, within the mesosphere/lower thermosphere (MLT) region.

For upper thermospheric altitudes (above 200 km) there have been only a few studies on global GW climatology. *Bruinsma and Forbes* [2008] investigated dependences of GW climatology on geomagnetic/solar activity, local time (LT), and latitude, while the seasonal and longitudinal variations were not addressed. *Potter et al.* [1976] and *Hedin and Mayr* [1987] focused mainly on high-latitude regions, where strong atmospheric fluctuations occur in connection with auroras, while the midlatitude/low-latitude GWs were not discussed in detail. Although *Hedin and Mayr* [1987, Figure 2] show global maps of GW activity, questions remain: (1) the contour levels at midlatitudes/low latitudes are too coarse to draw much information from them and (2) all the seasons are mixed in one map. In this study we report, for the first time, a detailed seasonal/geographical GW climatology in the upper thermosphere at geomagnetically midlatitudes/low latitudes. We use the data from the Challenging Minisatellite Payload (CHAMP) satellite mission at an altitude ~300–400 km from June 2001 to September 2010.

2. Observation

The CHAMP satellite was launched in July 2000 into a polar, circular orbit. The altitude was initially about 450 km, which gradually decayed until the final atmospheric reentry in September 2010. The satellite needed about 130 days to collect data from all LT sectors. CHAMP carried an accelerometer (ACC) [e.g., *Bruinsma and Biancale*, 2003] from which averaged neutral mass density is deduced every 10 s [e.g., *Bruinsma et al.*, 2004; *Liu et al.*, 2005; *Doornbos et al.*, 2010].

This corresponds to a distance of ~75 km (considering the orbital speed of 7.5 km/s). To extract a GW climatology as reliably as possible, we use the following criteria for event selection. First, we omit nighttime ACC data because they may contain signatures of equatorial plasma bubbles [e.g., *Illés-Almár et al.*, 1998; *Park et al.*, 2010]. Further, we avoid data between 06 and 08 LT because the low background level [e.g., *Liu et al.*, 2005, Figure 2a], in combination with the accuracy of CHAMP/ACC density estimates (about 1×10^{-14} kg/m^3 [*Liu et al.*, 2005]), can result in artificial fluctuations. This is in particular true for time around June solstice at solar minimum. We focus on the daytime sector covering the LT range of 09–18 LT.

Figure 1 illustrates our data processing method. In Figure 1 (top) the black solid curve represents the neutral mass density (ρ) as recorded by the CHAMP/ACC. A Savitzky-Golay low-pass filter (order = 3, window size = 11 data points) is applied to the recordings to yield a smooth background density (ρ_{mean}, Figure 1, red curve). Figure 1 (middle) shows density variations ($\delta\rho$) which are differences between the black and red curves in Figure 1 (top). The resulting passband of along-track scale length in the density variations spans approximately 150 km to 600 km. The lower bound (150 km) represents the Nyquist limit due to the sampling cadence while the upper bound (600 km) was chosen to reject effects of large-scale traveling ionospheric/atmospheric disturbances, whose horizontal wavelength is above 1000 km [e.g., *Shiokawa et al.*, 2005]. This horizontal wavelength range is also comparable to two of the key references, *Ern et al.* [2011] and *John and Kumar* [2012] ($\lambda_h >$ ~200 km), which address GW activity both within and above the stratosphere. Figure 1 (bottom) presents density variations normalized by the background density (i.e., $\delta\rho/\rho_{\mathrm{mean}}$).

For our global climatology we divide the world map into bins of 5° in geographic latitude (GLAT) by 5° in GLON. The bin size in GLAT approximately corresponds to six consecutive data points of the CHAMP/ACC. Inside each bin $|\delta\rho/\rho_{\mathrm{mean}}|$ is averaged to represent the GW activity level. The resultant global map is smoothed further by a 3 by 3 median filter. Separate global maps are obtained for the three Lloyd seasons: combined equinoxes, June solstice, and December solstice. For each season ~131 days have been considered, which are centered on the respective equinox and solstice epochs. In this way we guarantee uniform LT coverage for each season. Note that CHAMP/ACC data during disturbed periods ($K_p > 4.0$) are omitted here.

3. Results

Figure 2 shows global maps of the GW activity for the three different seasons: equinoxes, June solstice, and December solstice. On average, there are more than 600 data points per bin. The color bar is scaled logarithmically, and gray represents the lowest level of the color scale. The dashed lines show geomagnetic latitudes (MLAT). The dayside (09–18 LT) data set from 2006 to 2010 (representing solar minimum conditions) was used for Figure 2. Note the extremely high GW activity at high latitudes, which agrees with findings of *Potter et al.* [1976] and *Hedin and Mayr* [1987]. Density undulations due to substorms on the nightside [e.g., *Ritter*

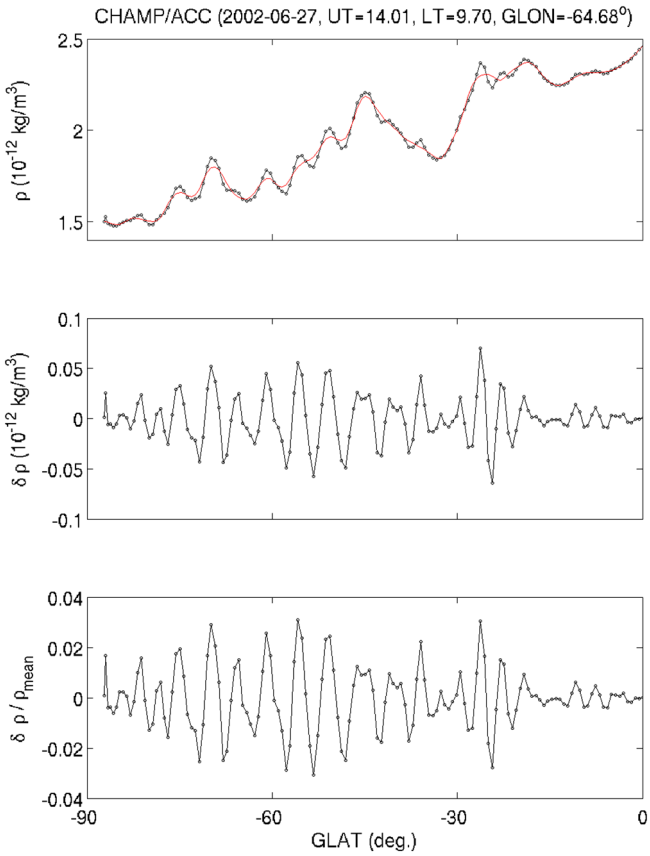

Figure 1. An illustration of our data processing method. (top) The black solid curve shows the neutral mass density as recorded by the CHAMP/ACC, while the red curve represents background density. (middle) Density variations, which are the differences between the black and red curves in Figure 1 (top). (bottom) Density variations normalized by the background density.

et al., 2010] and/or from the cusp density anomalies [e.g., *Lühr et al.*, 2004] may contribute to the high-latitude GW signals. Our study therefore focuses on midlatitude/low-latitude regions. Notable features in Figure 2 can be summarized as follows. First, high GW activity at midlatitudes appears in the winter hemisphere. During local winter at midlatitudes GW activity shows much stronger longitudinal variations in the Southern than the Northern Hemisphere. Second, GW activity near Andes and Antarctic Peninsula during June solstice (Figure 2, second panel) is higher than in any other season or location. Third, GW activity in the low-latitude (±30° GLAT) summer hemisphere is stronger above continents than over oceans. This trend is clearer during December solstice and equinoxes than during June solstice.

We also constructed GW climatology maps during solar maximum (2001–2005), which are shown in Figure 3. These show similar morphologies as during solar minimum. However, the overall relative GW amplitude at midlatitudes/low latitudes is ~2 times higher during solar minimum than solar maximum, which is qualitatively consistent with *Bruinsma and Forbes* [2008].

4. Discussion

4.1. Comparison With Stratospheric GW Climatology

The prime objective of this study is to extend the global GW surveys to the upper thermosphere. We first compare midlatitude regions of Figure 2 with stratospheric GW activity reported previously. For both upper thermospheric and stratospheric GWs the primary occurrence peak appears at midlatitudes of the winter hemisphere [e.g., *Ern et al.*, 2011; *John and Kumar*, 2012]. Around June solstice the global peak is focused near the Andes and Antarctic Peninsula, for both upper thermospheric and stratospheric GW [e.g., *Wu*, 2004; *Hoffmann et al.*, 2013]. Also, the GW activity around December solstice exhibits multiple peaks at various GLON sectors, for both upper thermospheric and stratospheric GW [*McLandress et al.*, 2000; *Jiang et al.*,

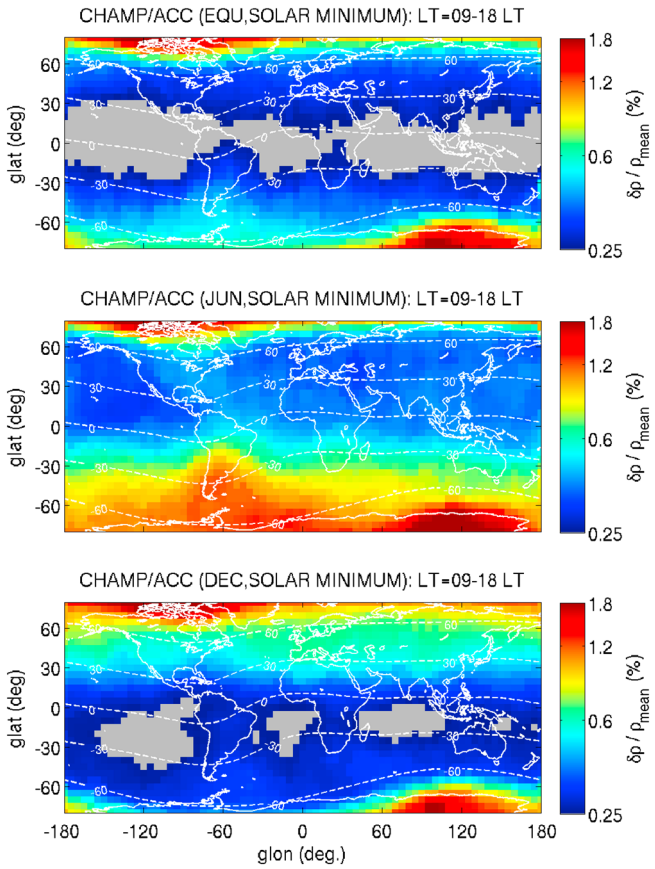

Figure 2. Global maps of the GW activity for equinox, June solstice, and December solstice during solar minimum years. The dashed curves represent geomagnetic latitudes.

2004]. Figure 4 presents a direct comparison between our Figure 2 and stratospheric GW climatology reproduced from *Jiang et al.* [2003, 2004]. Figure 4 (left column) represents June solstice and Figure 4 (right column) represents December solstice while Figure 4 (top row) corresponds to stratospheric GW climatologies and Figure 4 (bottom row) corresponds to upper thermospheric GW climatologies. In Figure 4 we can see that the GLON distribution of GW hot spots exhibits reasonable agreement with that in the stratosphere although the distribution in the upper thermosphere is not so confined in terms of latitude/longitude as in the stratosphere.

At the low-latitude summer hemisphere Figure 2 generally shows stronger GW activity above continents than above oceans. This trend is quite clear during December solstice. Although this trend is not as strong during June solstice at the low-latitude summer hemisphere, the GW activity is the lowest (highest) in the Pacific Ocean (above the American continent).

This trend is consistent with those from the stratospheric GW climatology although the latter is more confined latitudinally than the former [e.g., *Wu and Zhang*, 2004; *John and Kumar*, 2013]. *Vadas and Liu* [2013] demonstrated that thermospheric fluctuations are spread over a much wider spatial extent than the tropospheric source region. This may explain why the GW activity at the low-latitude (local) summer hemisphere in our Figure 2 does not show latitudinally confined features. Though GW amplitudes are somewhat enhanced over the continents, where the low-latitude stratospheric GW activity peaks [e.g., *Wu and Zhang*, 2004; *Gurvich et al.*, 2007], the mass density variation recorded by CHAMP at low latitudes are so small (on the order of 0.1% of the background; see Figures 2 and 3) that we cannot retrieve any details from them. Nevertheless, the general agreement between stratospheric (z ~20–60 km) and upper thermospheric (z ~300–400 km) GW distributions can be regarded as good for both midlatitude and low-latitude regions. Hence, neutral mass density fluctuations as observed by CHAMP at dayside midlatitudes/low latitudes

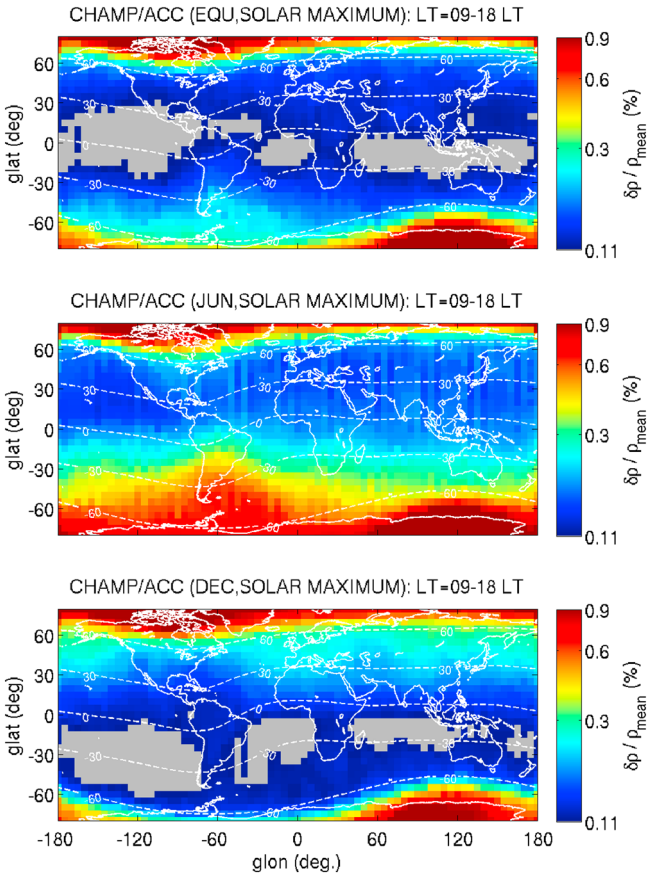

Figure 3. The same as Figure 2 but for solar maximum years. Note that the color scales are different from those of Figure 2.

appear to originate from tropospheric/stratospheric activity, via upward propagation of either original GWs or secondary waves generated subsequently.

The GW activity is higher during solar minimum than solar maximum when we use $\delta\rho/\rho_{mean}$ as GW activity proxy. Similar solar cycle dependence was found for GW momentum fluxes in the stratosphere, which is proportional to relative temperature fluctuations [*Ern et al.*, 2011]. For GWs satisfying the Boussinesq approximation the following equation holds $\delta\rho/\rho_{mean} = -\delta T/T_{mean}$ [*Vadas*, 2013]. Thus, results using $\delta T/T_{mean}$ should be similar to those using $\delta\rho/\rho_{mean}$. However, note in *Ern et al.* [2011] that the connection of stratospheric GW with solar activity is not so straightforward (only about 15% variation is observed) [see *Ern et al.*, 2011, Figure 8f]. Therefore, the very clear dependence of upper thermospheric GW on solar activity, as shown in our Figure 2 (variation by a factor of 2), cannot be explained fully by the dependence of stratospheric GW on solar activity. Rather, wave dissipation/propagation between the stratosphere and upper thermosphere, which changes significantly with solar cycle, seems to play an important role [e.g., *Yiğit and Medvedev*, 2010].

4.2. Comparison With GW Climatology at MLT Altitudes

The poor correlation between stratospheric and MLT GW climatology observed by the same instruments, as briefly reviewed in section 1, suggests that stratospheric GWs cannot directly penetrate up to upper thermospheric CHAMP altitudes with their horizontal wavelength preserved. One possible explanation is that stratospheric GWs create body forces in the MLT and thermosphere ($z \sim$150–250 km) via wave breaking and dissipation [e.g., *Fritts et al.*, 2002; *Vadas et al.*, 2003; *Vadas and Liu*, 2013, to name a few]. These processes excite secondary GWs with large horizontal phase speeds, thereby allowing them to propagate much higher into the thermosphere [*Vadas*, 2007]. Their initial amplitudes are small. Since their amplitudes grow nearly exponentially with altitude, this mechanism can allow the GW climatology in the upper thermosphere to reflect the stratospheric morphology.

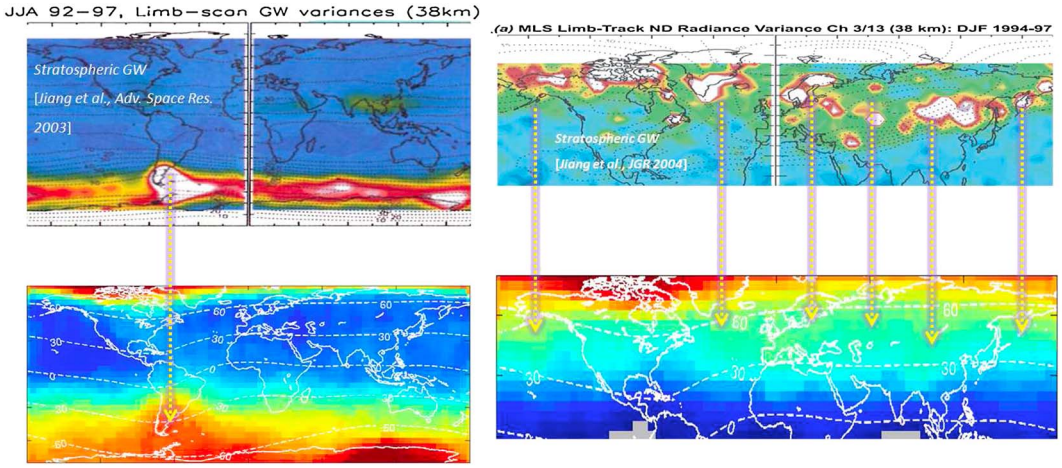

Figure 4. Comparison between Figure 2 and stratospheric GW climatology. (left column) June and (right column) December solstice while (top row) stratospheric and (bottom row) thermospheric GW climatology. Reprinted from *Jiang et al.* [2003, 2004] (with permission from Elsevier and John Wiley & Sons, respectively).

It is not known at what altitudes the global GW climatology (below CHAMP altitudes) starts to resemble the stratospheric distribution. Local observations can provide at least some clues. The King Sejong Station (KSS) is a Korean Antarctic station located at (62.221°S, 58.781°W), between the Andes and Antarctic Peninsula. Daily averaged variances of MLT horizontal winds have been acquired from the meteor radar observation since 2007 [*Lee et al.*, 2013]. We calculate monthly mean values of the daily variances (m^2/s^2) during local daytime (09–18 LT) and take the square root (m/s): hereafter, termed "KSS GW strength." This procedure is applied separately to different altitude ranges (between 82 km and 98 km) and different wind components (meridional and zonal). Similarly, for every CHAMP pass over KSS at local daytime we compute the variances of $\delta\rho$ (within a rectangular cell of $\pm 10°$ GLON and GLAT around the station) and calculate the square root of the mean monthly wave power: hereafter, 'CHAMP GW strength'.

Figure 5 presents the correlation between the KSS GW strength and the CHAMP GW strength from 2007 to 2009. The left (right) column shows zonal (meridional) MLT wind observed at KSS. Each row corresponds to a different (MLT) altitude. The correlation coefficient (R) between the KSS and CHAMP GW strengths is shown in each panel. Correlation coefficients are very low below 90 km altitude but increases significantly above 90 km. We have performed a Student's t test to evaluate the significance. The number of data points in each panel of Figure 5 is 18, which means that the degree of freedom is 16. If we set the one-tail alpha value to 0.1, the critical t value becomes 1.337. With respect to this critical t value all the correlations for $z < 90$ km become insignificant ($-0.60 \leq t$ value ≤ 0.92), while the correlations for $z \geq 90$ km are significant ($1.66 \leq t$ value ≤ 4.54) except for Figure 3 (bottom right) ($z = 98$ km, meridional wind; t value = 1.24). The t test results thus imply a significant change of GW climatology around the height level of $z = 90$ km, at least for the years 2007–2009 near the Andes/Antarctic Peninsula. Note that *Lee et al.* [2013, Figure 5] also show conspicuous differences in GW climatology below and above $z = 90$ km, further supporting our result. The fact that the correlation between KSS and CHAMP GW strengths peaks at 92 km (see our Figure 5) may imply GW dissipation and secondary GW generation at two different altitude regions (e.g., slightly below 90 km and around 140 km) as suggested by *Vadas and Crowley* [2010, Figure 14]. On the other hand, the number of meteor tails inherently exhibits a particular height distribution. The distribution peaks at 89–92 km in general [*Kim et al.*, 2012] although conspicuous difference between >90 km and <90 km altitudes, as seen in our Figure 5, does not exist [e.g., *Avery et al.*, 1983, Figure 2]. Hence, the data quality of the KSS GW strength is expected to be highest around 89–92 km altitude [e.g., *Vincent et al.*, 2010], which may also affect the degree of correlation between the KSS and CHAMP GW strengths. More observations with various instruments are needed to determine (1) whether GW climatology remains nearly the same throughout the altitudes between 90 km and 300 km and (2) whether the results in our Figure 5 also hold for other geographic locations and time periods.

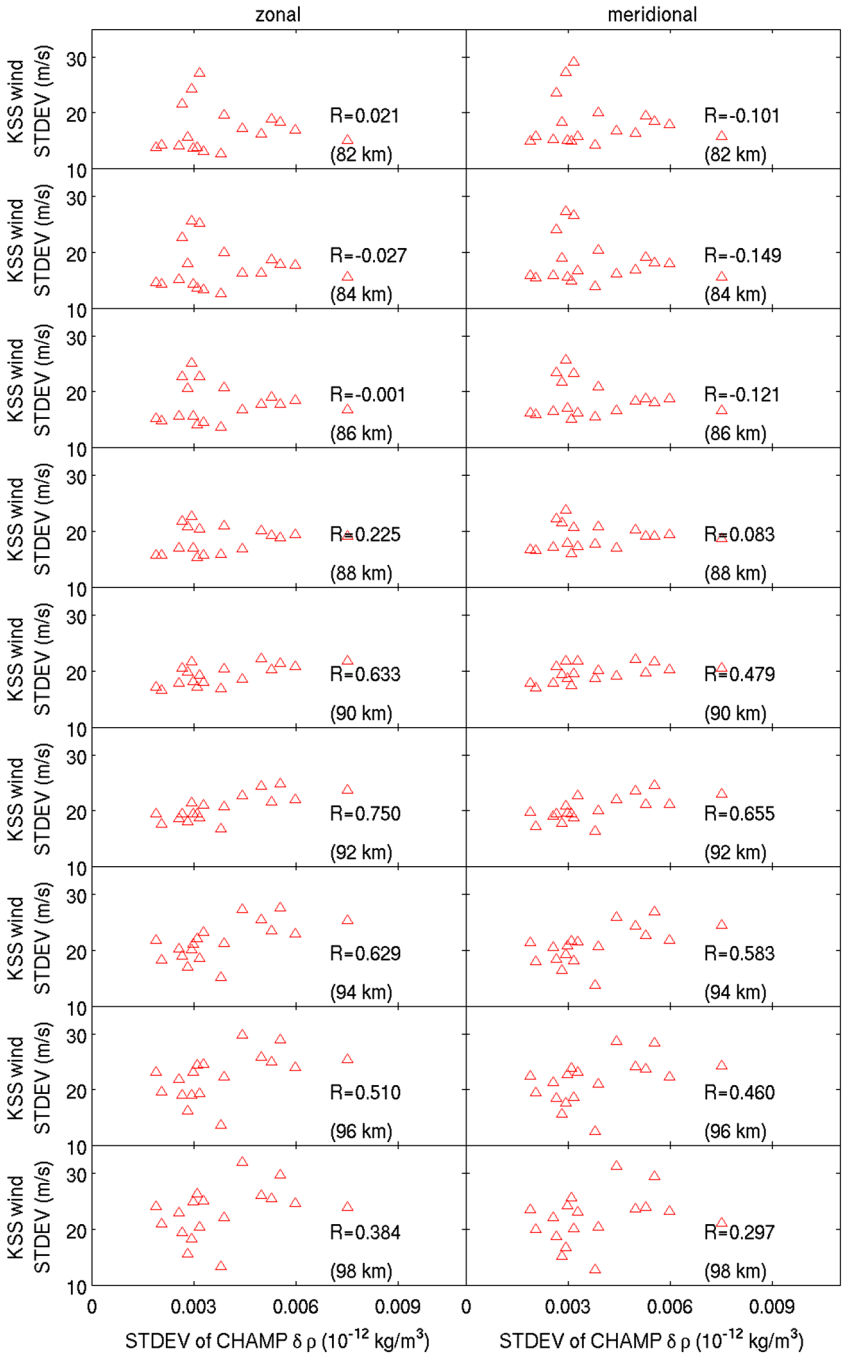

Figure 5. Correlation coefficients (*R*) between the KSS GW strength and the CHAMP GW strength from 2007 to 2009. The left (right) column presents zonal (meridional) MLT wind. Each row corresponds to a different altitude range.

4.3. Effects of Background Plasma Density

Figure 6 has the same format as Figure 2 but shows bin averages of background plasma density measured by the Planar Langmuir Probe (PLP) on board CHAMP. We can see that regions of very low plasma density (on the order of 10^4 cm^{-3}) in Figure 6 are in the winter hemisphere. Moreover, the plasma density around the Andes and Antarctic Peninsula during June solstice is lower than that in any other location and season. These features of plasma density agree with those of midlatitude GW hot spots as shown in Figure 2. It would be worth studying whether there is a causal relation of low plasma density regions with the common GW hot spots in the stratosphere and upper thermosphere. Because the *F* region plasma is tightly bound

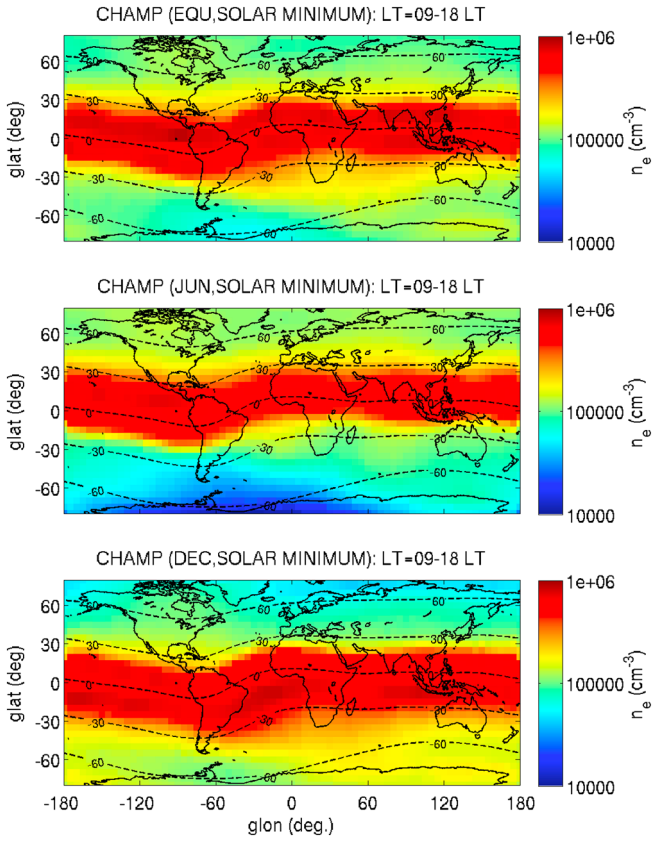

Figure 6. The same as Figure 2 but for bin averages of background plasma density observed by the CHAMP/PLP.

to geomagnetic field lines, it can act as a damping obstacle for fluctuations of upper thermospheric density due to ion/neutral collisions.

It would have been interesting to check undulations of ionospheric plasma density using the CHAMP/PLP: a number of previous studies [e.g., *Vadas and Crowley*, 2010; *Otsuka et al.*, 2013; *Nishioka et al.*, 2013] suggested that thermospheric GWs can generate undulations of ionospheric plasma density. However, plasma density undulations around the GW hot spots in Figure 2 can fall below the sensitivity limit of the instrument (about 10^3 cm^{-3}, figure not shown). In particular, near the Antarctic Peninsula the undulations of recorded plasma density seem to be governed by this instrument noise. We thus could not derive a reliable climatology of plasma density fluctuations related to the upper thermospheric GWs. Instead we compare our results to published climatologies of plasma density fluctuations, such as dayside medium-scale traveling ionospheric disturbances (MSTIDs). Using ground-based observations of total electron content, *Kotake et al.* [2006] and *Otsuka et al.* [2013] reported that dayside MSTIDs preferentially occur during local winter. These results are consistent with the upper thermospheric GW climatology in our study, which supports their speculation that the GWs are the source of daytime MSTIDs. However, daytime MSTIDs are not significantly affected by solar activity [*Kotake et al.*, 2006], and the seasonal variation amplitude near South America is not much larger than in other GLON sectors [*Kotake et al.*, 2006, Figure 4]. Both of these results are at odds with ours. Hence, it is not easy to find a one-to-one correspondence between our results (the GW climatology in the dayside upper thermosphere) and ground-based dayside MSTID climatologies published previously. This topic should be pursued in depth by future missions with more sensitive plasma density measurements and global coverage.

5. Summary

In this study we investigated the medium-scale (horizontal wavelength: 150–600 km) upper thermospheric GW climatology using the CHAMP mass density observations from 2001 to 2010. Our study mainly focuses

on the daytime (09–18 LT) and midlatitude/low-latitude upper thermosphere between 300 km and 400 km altitudes. The main conclusions can be summarized as follows:

1. Midlatitude GW activity is strongest in the winter hemisphere.
2. GW activity during June solstice adjacent to the Andes and Antarctic Peninsula is stronger than in any other season or location.
3. GW activity in the low-latitude summer hemisphere is stronger above continents than over oceans: especially during December solstice and equinoxes. However, density variations are so small that no detail can be derived from CHAMP observations.
4. In terms of relative density variation ($\delta\rho/\rho_{\mathrm{mean}}$), GW activity is twice as strong during solar minimum as during solar maximum.

   These results agree reasonably well with the characteristics of stratospheric GWs. Our observations imply that upper thermospheric GWs encountered by CHAMP mainly originate from the troposphere and/or stratosphere, either as primary or secondary GWs.

   Using MLT region wind variances at KSS (near Antarctic Peninsula) in 2007–2009, we investigated their correlation with CHAMP data:
5. The GW recordings from 90 to 98 km altitudes agrees better with CHAMP measurements, yielding significant correlations, than the observations from 82 to 88 km altitudes. This result supports the idea that the dissipation/breaking of primary GWs creates secondary GWs near the MLT; some secondary GWs can propagate into the midthermosphere/upper thermosphere because of their larger horizontal phase speeds while primary GWs mainly dissipate below [e.g., *Vadas*, 2007].

Acknowledgments

We sincerely thank S. Vadas for helpful discussions about gravity wave properties. The CHAMP mission was sponsored by the Space Agency of the German Aerospace Center (DLR) through funds of the Federal Ministry of Economics and Technology, following a decision of the German Federal Parliament (grant 50EE0944). The neutral wind data at KSS are provided by Korea Polar Research Institute (PE14010).

Robert Lysak thanks the reviewers for their assistance in evaluating this paper.

References

Alexander, M. J., et al. (2008), Global estimates of gravity wave momentum flux from high resolution dynamics limb sounder observations, *J. Geophys. Res.*, *113*, D15S18, doi:10.1029/2007JD008807.

Avery, S. K., A. C. Riddle, and B. B. Balsley (1983), The Poker Flat, Alaska, MST radar as a meteor radar, *Radio Sci.*, *18*(6), 1021–1027, doi:10.1029/RS018i006p01021.

Bruinsma, S., and R. Biancale (2003), Total densities derived from accelerometer data, *J. Spacecraft Rockets*, *40*(2), 230–236.

Bruinsma, S., D. Tamagnan, and R. Biancale (2004), Atmospheric densities derived from CHAMP/STAR accelerometer observations, *Planet. Space Sci.*, *52*(4), 297–312.

Bruinsma, S. L., and J. M. Forbes (2008), Medium- to large-scale density variability as observed by CHAMP, *Space Weather*, *6*, S08002, doi:10.1029/2008SW000411.

Doornbos, E., J. van den IJssel, H. Lühr, M. Förster, and G. Koppenwallner (2010), Neutral density and crosswind determination from arbitrarily oriented multiaxis accelerometers on satellites, *J. Spacecraft Rockets*, *47*(4), 580–589, doi:10.2514/1.48114.

Ern, M., P. Preusse, J. C. Gille, C. L. Hepplewhite, M. G. Mlynczak, J. M. Russell III, and M. Riese (2011), Implications for atmospheric dynamics derived from global observations of gravity wave momentum flux in stratosphere and mesosphere, *J. Geophys. Res.*, *116*, D19107, doi:10.1029/2011JD015821.

Fritts, D. C., S. L. Vadas, and Y. Yamada (2002), An estimate of strong local body forcing and gravity wave radiation based on OH airglow and meteor radar observations, *Geophys. Res. Lett.*, *29*(10), 1429, doi:10.1029/2001GL013753.

Gurvich, A. S., V. F. Sofieva, and F. Dalaudier (2007), Global distribution of C_T^2 at altitudes 30–50 km from space-borne observations of stellar scintillation, *Geophys. Res. Lett.*, *34*, L24813, doi:10.1029/2007GL031134.

Hedin, A. E., and H. G. Mayr (1987), Characteristics of wavelike fluctuations in dynamics explorer neutral composition data, *J. Geophys. Res.*, *92*(A10), 11,159–11,172, doi:10.1029/JA092iA10p11159.

Hoffmann, L., X. Xue, and M. J. Alexander (2013), A global view of stratospheric gravity wave hotspots located with atmospheric infrared sounder observations, *J. Geophys. Res. Atmos.*, *118*(2), 416–434, doi:10.1029/2012JD018658.

Illés-Almár, E., I. Almár, and P. Bencze (1998), Neutral density depletions attributed to plasma bubbles, *J. Geophys. Res.*, *103*(A3), 4115.

Jiang, J. H., D. L. Wu, S. D. Eckermann, and J. Ma (2003), Mountain waves in the middle atmosphere: Microwave limb sounder observations and analyses, *Adv. Space Res.*, *32*(5), 801–806, doi:lO.l016/S0273-1177(03)00402-2.

Jiang, J. H., S. D. Eckermann, D. L. Wu, and J. Ma (2004), A search for mountain waves in MLS stratospheric limb radiances from the winter Northern Hemisphere: Data analysis and global mountain wave modeling, *J. Geophys. Res.*, *109*, D03107, doi:10.1029/2003JD003974.

John, S. R., and K. K. Kumar (2012), TIMED/SABER observations of global gravity wave climatology and their interannual variability from stratosphere to mesosphere lower thermosphere, *Clim. Dyn.*, *39*, 1489–1505, doi:10.1007/s00382-012-1329-9.

John, S. R., and K. K. Kumar (2013), A discussion on the methods of extracting gravity wave perturbations from space-based measurements, *Geophys. Res. Lett.*, *40*, 2406–2410, doi:10.1002/grl.50451.

Kim, J.-H., Y. H. Kim, C. S. Lee, and G. Jee (2012), Mesospheric temperature estimation from meteor decay times of weak and strong meteor trails, *J. Atmos. Sol. Terr. Phys.*, *89*, 18–26.

Kotake, N., Y. Otsuka, T. Tsugawa, T. Ogawa, and A. Saito (2006), Climatological study of GPS total electron content variations caused by medium-scale traveling ionospheric disturbances, *J. Geophys. Res.*, *111*, A04306, doi:10.1029/2005JA011418.

Lee, C., Y. H. Kim, J.-H. Kim, G. Jee, Y.-I. Won, and L. W. Dong (2013), Seasonal variation of wave activities near the mesopause region observed at King Sejong Station (62.221S, 58.781W), Antarctica, *J. Atmos. Sol. Terr. Phys.*, *105-106*(2013), 30–38.

Liu, H., H. Lühr, V. Henize, and W. Köhler (2005), Global distribution of the thermospheric total mass density derived from CHAMP, *J. Geophys. Res.*, *110*, A04301, doi:10.1029/2004JA010741.

Lühr, H., M. Rother, W. Köhler, P. Ritter, and L. Grunwaldt (2004), Thermospheric up-welling in the cusp region: Evidence from CHAMP observations, *Geophys. Res. Lett.*, *31*, L06805, doi:10.1029/2003GL019314.

McLandress, C., M. J. Alexander, and D. L. Wu (2000), Microwave Limb Sounder observations of gravity waves in the stratosphere: A climatology and interpretation, *J. Geophys. Res.*, *105*(D9), 11,947–11,967, doi:10.1029/2000JD900097.

Nishioka, M., T. Tsugawa, M. Kubota, and M. Ishii (2013), Concentric waves and short-period oscillations observed in the ionosphere after the 2013 Moore EF5 tornado, *Geophys. Res. Lett.*, *40*, 5581–5586, doi:10.1002/2013GL057963.

Otsuka, Y., K. Suzuki, S. Nakagawa, M. Nishioka, K. Shiokawa, and T. Tsugawa (2013), GPS observations of medium-scale traveling ionospheric disturbances over Europe, *Ann. Geophys.*, *31*, 163–172, doi:10.5194/angeo-31-163-2013.

Park, J., H. Lühr, and K. W. Min (2010), Neutral density depletions associated with equatorial plasma bubbles as observed by the CHAMP satellite, *J. Atmos. Sol. Terr. Phys.*, *72*(2-3), 157–163.

Potter, W. E., D. C. Kayser, and K. Mauersberger (1976), Direct measurements of neutral wave characteristics in the thermosphere, *J. Geophys. Res.*, *81*(28), 5002–5012, doi:10.1029/JA081i028p05002.

Preusse, P., et al. (2006), Tropopause to mesopause gravity waves in August: Measurement and modeling, *J. Atmos. Sol. Terr. Phys.*, *68*, 1730–1751.

Ritter, P., H. Lühr, and E. Doornbos (2010), Substorm-related thermospheric density and wind disturbances derived from CHAMP observations, *Ann. Geophys.*, *28*, 1207–1220, doi:10.5194/angeo-28-1207-2010.

Shiokawa, K., et al. (2005), Geomagnetic conjugate observation of nighttime medium-scale and large-scale traveling ionospheric disturbances: FRONT3 campaign, *J. Geophys. Res.*, *110*, A05303, doi:10.1029/2004JA010845.

Vadas, S. L., D. C. Fritts, and M. J. Alexander (2003), Mechanism for the generation of secondary waves in wave breaking regions, *J. Atmos. Sci.*, *60*, 194–214.

Vadas, S. L. (2007), Horizontal and vertical propagation, and dissipation of gravity waves in the thermosphere from lower atmospheric and thermospheric sources, *J. Geophys. Res.*, *112*, A06305, doi:10.1029/2006JA011845.

Vadas, S. L., and G. Crowley (2010), Sources of the traveling ionospheric disturbances observed by the ionospheric TIDDBIT sounder near Wallops Island on 30 October 2007, *J. Geophys. Res.*, *115*, A07324, doi:10.1029/2009JA015053.

Vadas, S. L. (2013), Compressible f-plane solutions to body forces, heatings, and coolings, and application to the primary and secondary gravity waves generated by a deep convective plume, *J. Geophys. Res. Space Physics*, *118*, 2377–2397, doi:10.1002/jgra.50163.

Vadas, S. L., and H.-L. Liu (2013), Numerical modeling of the large-scale neutral and plasma responses to the body forces created by the dissipation of gravity waves from 6 h of deep convection in Brazil, *J. Geophys. Res. Space Physics*, *118*, 2593–2617, doi:10.1002/jgra.50249.

Vincent, R. A., S. Kovalam, I. M. Reid, and J. P. Younger (2010), Gravity wave flux retrievals using meteor radars, *Geophys. Res. Lett.*, *37*, L14802, doi:10.1029/2010GL044086.

Wang, L., and M. J. Alexander (2010), Global estimates of gravity wave parameters from GPS radio occultation temperature data, *J. Geophys. Res.*, *115*, D21122, doi:10.1029/2010JD013860.

Wu, D. L., and J. W. Waters (1996), Gravity-wave-scale temperature fluctuations seen by the UARS MLS, *Geophys. Res. Lett.*, *23*, 3289–3292.

Wu, D. L. (2004), Mesoscale gravity wave variances from AMSU-A radiances, *Geophys. Res. Lett.*, *31*, L12114, doi:10.1029/2004GL019562.

Wu, D. L., and F. Zhang (2004), A study of mesoscale gravity waves over the North Atlantic with satellite observations and a mesoscale model, *J. Geophys. Res.*, *109*, D22104, doi:10.1029/2004JD005090.

Yiğit, E., and A. S. Medvedev (2010), Internal gravity waves in the thermosphere during low and high solar activity: Simulation study, *J. Geophys. Res.*, *115*, A00G02, doi:10.1029/2009JA015106.